Chapter 8
Model-Form Uncertainty in Predicting Electromechanical Passive and Active Damping Forces for a One-Mass Oscillator

Murali Krishnan Mohan Kumar and Roland Platz

Abstract This study investigates the passive and active damping behavior achieved by a voice coil actuator (VCA) for a one-mass oscillator subjected to passive and active vibration isolation. The novelty of this investigation lies in validating an adequate analytical model that predicts the passive and active damping properties provided by the VCA for the one-mass oscillator. In the existing analytical model, the VCA forces are functions solely of the passive damping coefficients as well as active gains and the velocities of the mass from a velocity feedback control to realize active damping. Initial verification and validation reveal discrepancies between the simulated numerical results and the experimental data. Experimentally, in higher damping scenarios, the resonance frequency of the one-mass oscillator shifts to higher values, whereas theoretically, it is expected to shift to lower values. The authors assume that the VCA's real behaviour is responsible for the shift. This motivates the following investigation. This study incorporates the electromechanical coupling of the VCA's inductance, resistance, and force constant with the mechanical damping and stiffness properties of the oscillator into the model.

Keywords Model-form uncertainty · Vibration isolation · Active and passive damping · Voice coil actuator · Electromechanical model

Introduction

Model-form uncertainties occur when there is ambiguity in establishing a functional relationship between the input and output of the model. This ambiguity can stem from unknown, incomplete, inadequate, and unreasonable functional relationships between the inputs and the corresponding responses or model parameters and internal variables of the model. This model-form discrepancy results in incompleteness in defining the scope of application of the model, [1]. Hence, identification and quantification of uncertainty associated with a mathematical model helps in model selection and offers a comparison of their discrepancies. Such a comparison aids a designer in deciding the adequacy of a simple model over a complex model with unacceptable or acceptable uncertainty, [2].

An analytical one-mass oscillator model, as outlined in [2], was used as the basis for the initial investigations into uncertainty in passive and active vibration reduction. This study examined vibration isolation, distinguishing passive damping which relies on inherent system parameters such as inertia, stiffness, and damping and active damping, which uses additional controlled forces to enhance vibration isolation. Lenz and Platz [3] explored parametric uncertainty and validated the model with a test rig using an area validation matrix. Platz [2] identified the discrepancies between numerical one-mass oscillator and experimental results by the validation of the model for various damping cases. Further, a deterministic calibration of the one-mass oscillator along with a two-mass and a finite element (FE) model, representing the same experimental test set up was carried out in [4], keeping the damping ratio and stiffness as calibration parameters. [5] presented a mathematical model of a voice coil motor using the expression for LORENTZ FORCE incorporating the magnetic field density, current and geometric parameters of the coil. Banik et al.[6] optimised the design of a voice coil motor that can be used as an actuator for vibration isolation applications. The VCA model presented in [7], based on the Skyhook damper concept, was used for active vibration isolation using velocity feedback control. The electromechanical model of a one-mass oscillator in [8] accounts for the electromotive force of the actuator by considering its equivalent electric circuit parameters. Perfetto et al.[9] presented and validated a model of an active vibration absorber using a VCA with voltage driven feedback controller. This study investigated the actuator force, taking into account the electrical impedance of the VCA.

Murali Krishnan Mohan Kumar · Roland Platz
Department of Mechanical Engineering and Mechatronics, Deggendorf Institute of Technology, 91781 Weissenburg, Bavaria, Germany
e-mail: murali.mohan-kumar@th-deg.de; roland.platz@th-deg.de

Roland Platz et al. (eds.), *Model Validation and Uncertainty Quantification, Vol. 3*, Conference Proceedings of the Society for Experimental Mechanics Series, https://doi.org/10.13052/97887-438-0148-1_8

As an initial step to understand the discrepancies between the simulated results and experimental observations, the control voltage that creates the damping force generated by the VCA in the experimental test rig are examined in this paper. In the experiments, passive and active damping are realized through the control voltage of the VCA. However, the existing one-mass oscillator model treats the damping forces as pure mechanical forces, which are functions of the damping coefficient, active gain, and the velocities of the frame and mass. This work focuses on identifying discrepancies in the damping force predicted by the one-mass oscillator by incorporating electrical parameters, such as resistance, inductance, and the force constant of the VCA, based on the measured voltage values.

Formulation of the Analytical One-Mass Oscillator Model and Realized Test Rig

The one-mass oscillator model is a single degree of freedom system as described in [2]. It serves as the foundation for investigations aimed at evaluating model-form uncertainty in passive and active vibration reduction. In an application scenario, the model represents a suspension leg as illustrated in Figure 1a.

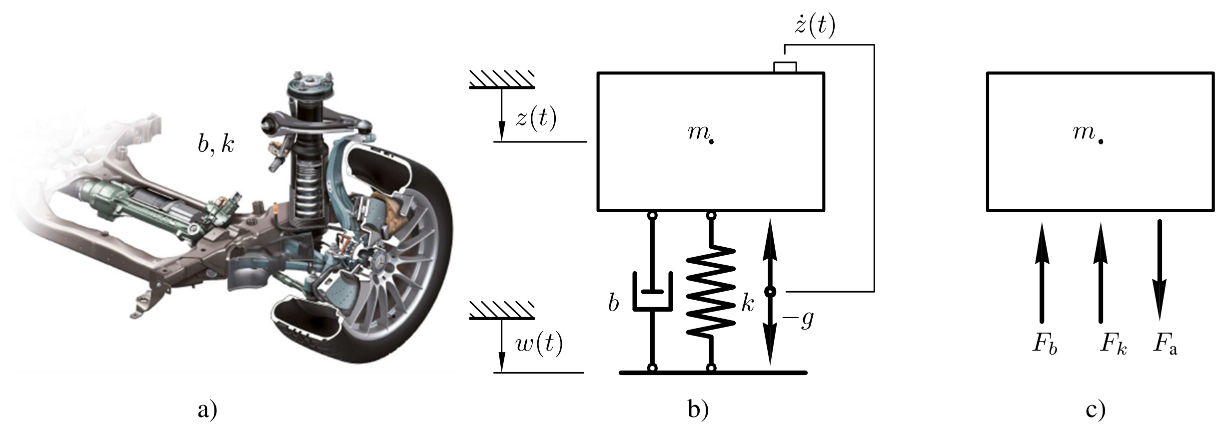

Fig. 1 Motivation for one-mass oscillator model from, a) front suspension leg (Mercedes Benz) with damping b and stiffness k, b) one-mass oscillator model with base excitation and active vibration isolation by active velocity feedback control, c) the passive and active forces acting on the oscillating mass,[3]

The suspension is modelled as a one-mass oscillator model in Figure 1b, where the passive configuration is characterized by the chassis mass m representing one quarter of a car, the stiffness k, and the damping coefficient b of the suspension leg, which is considered massless. In the active configuration, an additional velocity feedback gain g is introduced. The mass experiences an absolute vertical displacement $z(t)$ in response to a base point displacement excitation function $w(t)$. The base point, assumed to have no inertia, is represented by a horizontal line in Figure 1b. According to the principle of linear momentum, from Figure 1c

$$m\,\ddot{z}(t) = F_\mathrm{a} - F_b - F_k \tag{1}$$

where

$$F_\mathrm{a} = -g\,\dot{z}(t),\;\; F_b = b\,[\dot{z}(t) - \dot{w}(t)],\;\text{and}\; F_k = k\,[z(t) - w(t)] \tag{2}$$

are the active damping force, passive damping force, and stiffness force, respectively. The active force due to actuation arises from the velocity feedback, while the passive damping force depends on the passive damping coefficient b and the relative velocity $\dot{z}(t) - \dot{w}(t)$ between the mass and the frame.

From (1) and (2), the equation for equilibrium of forces becomes

$$m\,\ddot{z}(t) + (b+g)\,\dot{z}(t) + k\,z(t) = b\,\dot{w}(t) + k\,w(t). \tag{3}$$

The inhomogeneous differential equation of motion

$$\ddot{z}(t) + \left[2\,D_\mathrm{p}\,\omega_0 + \frac{g}{m}\right]\dot{z}(t) + \omega_0^2\,z(t) = 2\,D_\mathrm{p}\,\omega_0\,\dot{w}(t) + \omega_0^2\,w(t) \tag{4}$$

uses the passive damping ratio D_p and the angular eigen frequency ω_0 with

$$2D_\mathrm{p}\,\omega_0 = \frac{b}{m} \text{ and } \omega_0^2 = \frac{k}{m}.$$

The passive and active damping forces resulting from (3) are $2D_\mathrm{p}\,\omega_0\,m\,(\dot{z}-\dot{w})$ and $g\,\dot{z}$.

In the automotive application scenario illustrated in Figure 1a, the base point excitation $w(t)$ in Figure 1b ideally represents driving on an uneven road. To simulate this condition in an experimental setup, an additional frame structure with mass m_f, damping coefficient b_f, and stiffness k_f was incorporated into the test rig, Figure 2, [2] and [4]. In the actual test setup, the single-mass oscillator is mounted within a frame of relatively large mass m_f compared to m. The model parameters used for the test rig are detailed in Table 1. The setup acts as the physical embodiment of the one-mass oscillator system shown in Figure 1b. A modal hammer applies the force on the frame, Figures 2a and 2b. It is then converted into a displacement excitation of the frame mass m_f. The test rig is supported by an elastic foundation with relatively low damping b_f and low stiffness k_f, Figure 2. The assumed damping coefficient b_f, with the corresponding damping ratio D_f = 0.1 %, and the stiffness k_f are relatively small compared to the damping ranges b, with the corresponding damping ratio D between 12 and 28 %, and the stiffness ranges k of the leaf springs, Table 1. This results in a quasi-static dynamic response of the frame following the hammer impact, characterized by a relatively low first eigenfrequency $\omega_{0,\mathrm{f}} \approx 2\pi\,1/\mathrm{s}$, which is much lower than the first eigenfrequency ω_0 of mass m.

Table 1 Values of parameters used for the analyses, [4]

Model parameters	Variables	Realized values	Unit
oscillating mass	m	0.79 – 1.60	kg
damping coefficient	b	39 – 93	Ns/m
stiffness	k	25,788 – 38,494	N/m
gain	g	15 – 84	Ns/m
frame mass	m_f	10	kg
frame damping coefficient	b_f	0.17	Ns/m
frame stiffness	k_f	722	N/m
eigenfrequency	ω_0	(26.2 –36.7) $\cdot\,2\pi$	1/s

Figure 2a presents a schematic of the test rig. The rigid frame features two supports that secure a leaf spring at points A and C. The effective bending lengths on sides A–B and B–C are denoted as *l*, with the oscillating mass *m* positioned at

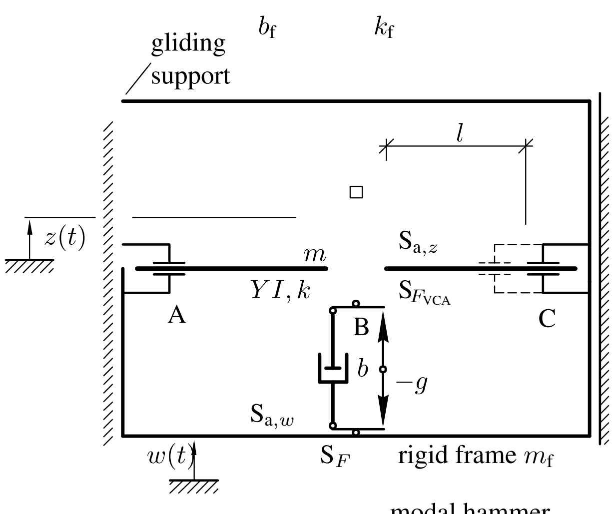

Fig. 2 a) Concept of the experimental realization for vibration isolation – schematic diagram of the real test set up; b) realized test rig, [2]

the center point B. The leaf spring has a cross-sectional area of $d\,h$, defined by its width d and height h. Its stiffness k is determined by the bending stiffness *EI*, where E represents the Young's modulus of the carbon fiber reinforced polymer (CFRP) used for the leaf spring, and I is the area moment of inertia. The two supports at A and C can be adjusted along l to fine-tune the leaf spring's bending deflection and, consequently, its effective stiffness k. A VCA generates the passive and active damping forces F_b, F_a introduced in (2) and in Figure 1c. The force sensor $\mathrm{S}_{F_\mathrm{VCA}}$ at B captures the sum of the forces F_a + F_b acting on the oscillating mass, Figure 2a.

Responses from the experimental tests are recorded using acceleration and force sensors S_a and S_F. Figure 2a illustrates the accelerometers $\mathrm{S}_{\mathrm{a},z}$ and $\mathrm{S}_{\mathrm{a},w}$, which measure the accelerations of the oscillating mass m and the frame mass m_f, respectively. The force sensor $\mathrm{S}_{F_\mathrm{VCA}}$ captures the damping force between m and m_f, while the force sensor S_F measures the force generated by the hammer impulse. The signals from these sensors are processed in the time domain using a real-time interface controller, along with high-pass/low-pass filters and a computer workstation, [2].

Modelling of the Voice Coil Actuator

Figures 3, 4, and 5 illustrate various components of VCA on the experimental test rig. A VCA works on the principle of electromagnetism, where the interaction between an electric current in a coil and a magnetic field generates linear forces [8]. The VCA enables the passive damping and active gain forces F_b and F_a during the experiments, Figure 3. The VCA consists of two primary components. The first component is a stationary cylindrical permanent magnet with an outer ring, which is affixed to the frame as the north pole (N), accompanied by a centered pole piece that serves as the south pole (S), Figures 4 and 5. The second component is a coil wound around a hollow, movable cylindrical mount that fits into the gap between the north and south poles of the magnet. A small air gap of approximately 1 to 1.5 mm exists between the magnet's poles and the cylindrical mount containing the coil, Figure 4. This cylindrical mount with the coil can move freely along the fixed z-axis between the north and south poles of the magnet, [2]. An applied control voltage regulates the current flowing through the coils within the magnetic field, resulting in the motion of the cylindrical mount in z-direction.

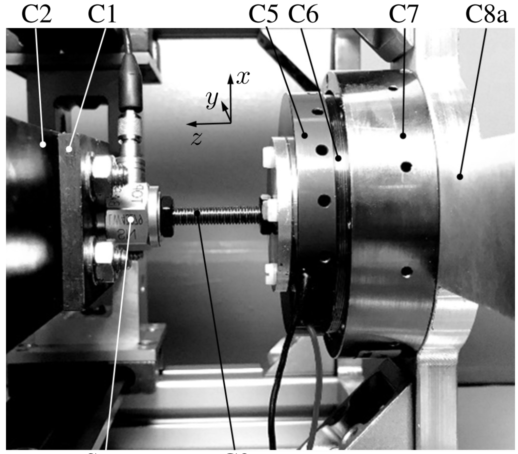

Fig. 3 VCA on the test rig: C1 rigid oscillating mass m, C2 one leaf spring with stiffness k/4, C3 fixed leaf spring support, C4 glide support, C5 VCA coil body, C6 VCA coil, C7 VCA stator, magnet outer ring, north pole, C8a front structure of rigid frame with mass m_f, C9 rigid coupling screw, $\mathrm{S}_{F_\mathrm{VCA}}$ force sensor to measure the sum of damping forces F_b and F_a

The magnet in Figure 4 provides a magnetic flux density $\vec{B}$, an electrical current $\vec{i}$ runs through the coil when applying a control voltage u. Both $\vec{B}$ and $\vec{i}$ are circumferential vectors around the z-axis with magnitude and direction. With the given direction of the current $\vec{i}$ in the plan view A-A in Figure 4, the LORENTZ force vector, [5] and [10],

$$\vec{F}_\mathrm{VCA} = r\,l\,\vec{i} \times \vec{B} \tag{5}$$

is given by the cross product of the current vector $\vec{i}$, multiplied by the length of the coil l and the ratio r of the effective length, and the magnetic flux density vector $\vec{B}$. Since $\vec{i} \perp \vec{B}$, the LORENTZ force becomes a scalar, [6],

$$F_\mathrm{VCA} = r\,l\,i \cdot B = \Psi\,i \tag{6}$$

with the force constant Ψ. In this work, this LORENTZ force is the electromotive force which accounts for the passive and active gain forces in (2), [2]. Hence,

$$F_{\text{VCA}} = b(\dot{z} - \dot{w}) + g\dot{z} = \Psi\, i. \tag{7}$$

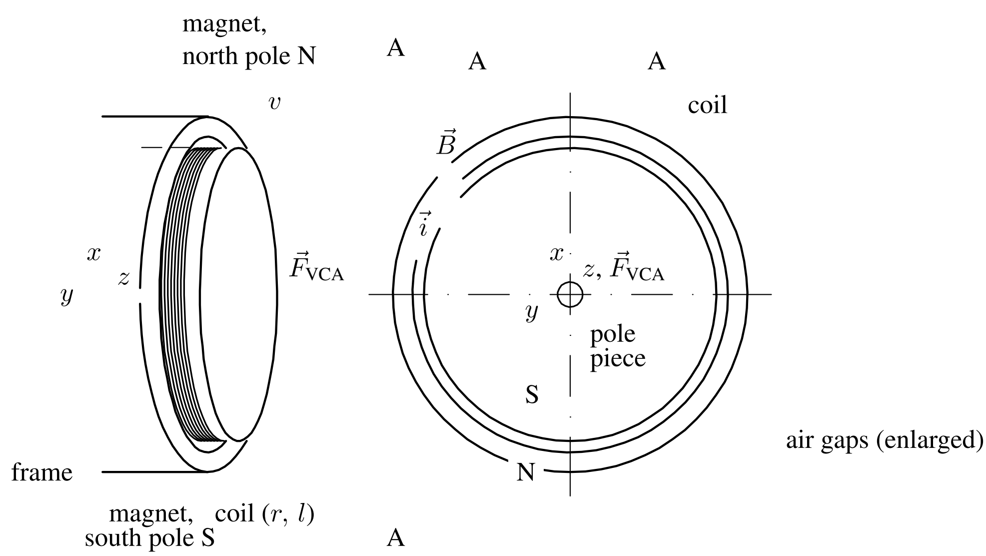

Fig. 4 Principal assembly of the VCA

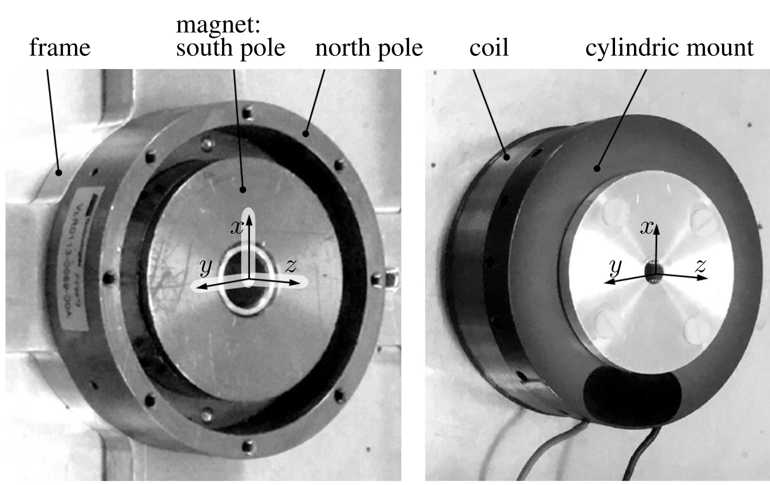

Fig. 5 Photo of VCA used in the rig

The driving electrical power of the VCA is

$$P = u_{\text{VCA}}\, i = F_{\text{VCA}}\, v \tag{8}$$

obtained by multiplying the current i with the driving voltage u_{VCA}. This is equivalent to the driving mechanical power, which can be expressed as the product of the electromotive force F_{VCA} and the velocity v of the coil's movement in the z-direction, Figure 4.

The electric equivalent circuit diagram of the VCA in Figure 6, [2] and [8], helps to understand the relation between the electrical and the mechanical quantities to, eventually, determine the electromotive force F_{VCA} (7) from an applied control voltage u. The VCA's properties are the inductance L, the Ohmic resistance R, and the force constant Ψ. Using the mesh rule, the applied control voltage becomes

$$u = u_{\text{VCA}} + u_{\text{L}} + u_{\text{R}}. \tag{9}$$

The voltages at L and R are

$$u_L = \frac{\mathrm{d}i}{\mathrm{d}t} L \ \ and \ u_R = iR, \tag{10}$$

and at Ψ, the driving voltage

$$u_{\text{VCA}} = \Psi\, v \tag{11}$$

initiates the electromotive force F_{VCA}.

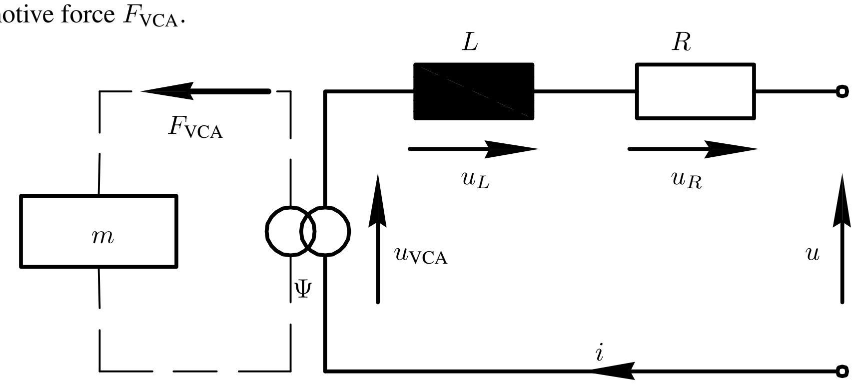

Fig. 6 Equivalent circuit of VCA to provide the electromotive force F_{VCA} as damping and active forces on the vibrating mass m

Hence, the first order differential equation determines the applied control voltage

$$u = \Psi\, v + \frac{\mathrm{d}i}{\mathrm{d}t} L + iR \tag{12}$$

as the sum of all voltages in the circuit in Figure 6. From (7), current

$$i = \frac{1}{\Psi}(b(\dot{z} - \dot{w}) + g\dot{z}) \tag{13}$$

is expressed in terms of force constant Ψ, the relative velocity between the magnet, which is fixed to the frame, and the coil winding, which is fixed to the moving mass m. The control voltage becomes, [2],

$$u = \left\{ \Psi(\dot{z} - \dot{w}) + \frac{\mathrm{d}}{\mathrm{d}t}\left[\frac{1}{\Psi}(b(\dot{z} - \dot{w}) + g\dot{z})\right] L + \frac{1}{\Psi}(b(\dot{z} - \dot{w}) + g\dot{z}) R \right\}. \tag{14}$$

This equation is analogous to the equation for voltage generated by feedback control, as suggested by [9], where the control voltage is represented as the sum of three contributions, each given by a gain multiplied by velocity. The first term, $\Psi(\dot{z} - \dot{w})$, represents the compensator, which is necessary to eliminate the effects of a back electromotive force between the coil and the magnet, [9].

Validation of Control Voltage Using Simulated and Experimental Comparisons

To validate the control voltage (14), calibrated values of the damping coefficient b, active gain g, and stiffness k from the one-mass oscillator in Figure 1 according to [4] are used. The simulated voltages from the model are compared with the measured control voltage obtained from experimental tests conducted for combinations of the mass m = 0.7853 kg and three damping cases D = 12%, 20% and 28%, Figure 7, for stiffness values

a) $k = 25,788$ N/m and
b) $k = 38,494$ N/m.

The gain is set to zero, g = 0, only passive cases are considered.

The comparison between the simulated and experimental control voltages in Figure 7 reveals deviations, particularly in amplitude across all cases. The simulated voltage appears to be a scaled version of the actual voltage, especially for the lowest and highest passive damping ratios of 12% and 28%. In the case of the 20% damping ratio, the results show deviations in both amplitude and phase. It can also be observed that the experimental values for the 20% and 28% damping ratios are in

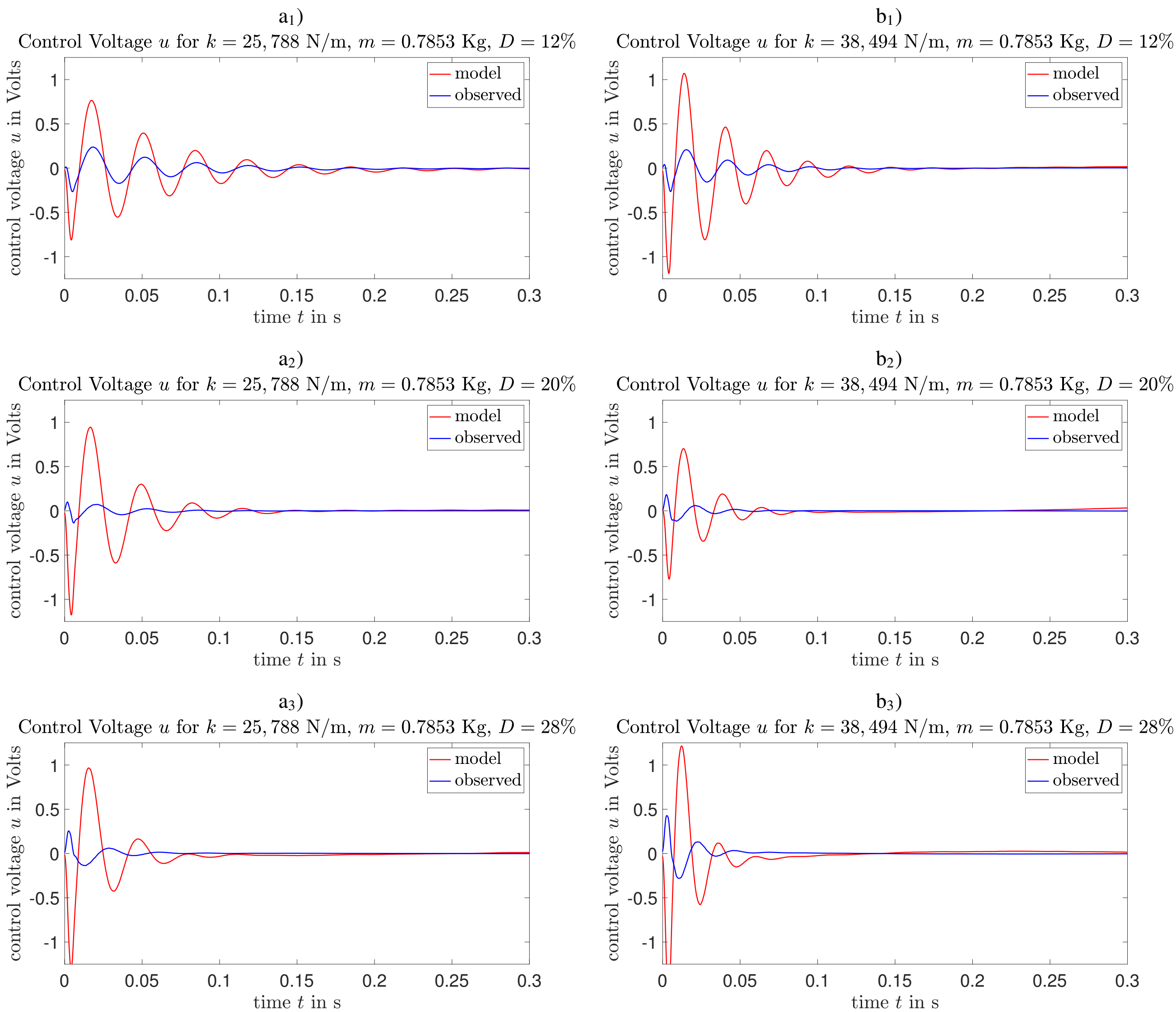

Fig. 7 Comparison of the observed control voltage and the model predictions for a) k = 25,788 N/m, and b) k = 38,494 N/m for the mass m = 0.7853 Kg and passive damping ratios D = 12%, 20%, 28%

Table 2 Suggested scale of simulated control voltage amplitudes in comparison to observed values

Damping Cases	k = 25,788 N/m, m = 0.7853 kg	k = 38,494 N/m, m = 0.7853 kg
	Scale	Scale
D_1 = 12%	2.55	8.07
D_2 = 20%	-6.87	-15.00
D_3 = 28%	-8.43	-4.45

reverse phase with the curve for the 12% damping ratio. However, the simulated curve for all three damping cases initially proceeds into the negative region and follows a similar trend.

A scaling factor for the amplitude is suggested in each case to match the model with the observations, Table 2. The values do not show a consistent trend across the passive damping ratios for the two test cases, though. Figure 8 shows the scaled plot of the simulated control voltage in comparison to the experimentally observed values. The scaled plot almost fits for the lowest and the highest damping values in both test cases. For the intermediate damping of 20%, adequate fit is not possible.

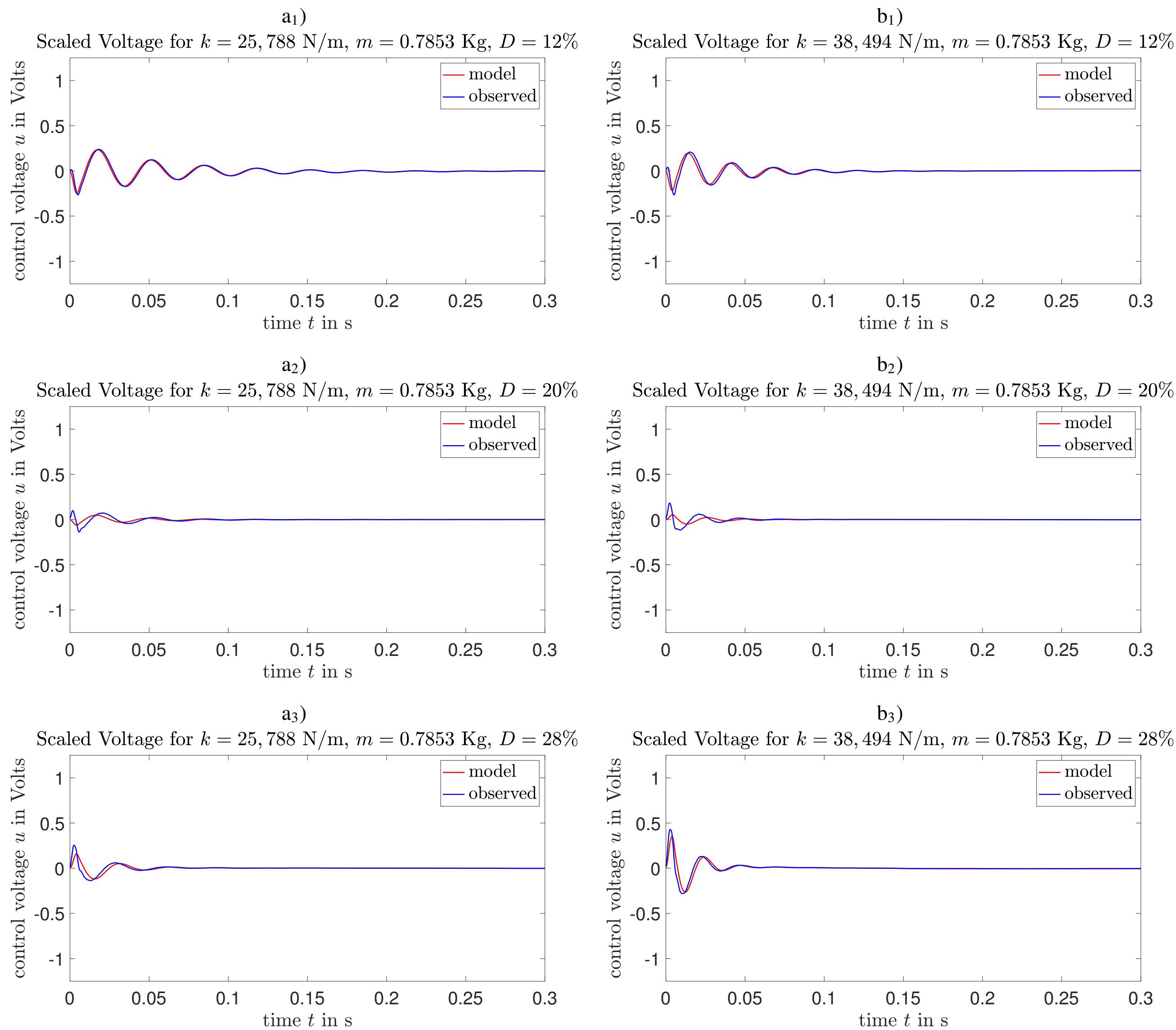

Fig. 8 Comparison of the observed control voltage and the scaled model predictions for a) k = 25,788 N/m, and b) k = 38,494 N/m for the mass m = 0.7853 Kg and passive damping ratios D = 12%, 20%, 28%

Conclusion

To reduce and identify model-form uncertainty in predicting the dynamic response of an analytical one-mass oscillator model, a VCA providing passive and active vibration isolation in the test rig was thoroughly investigated. An electromechanical model of the VCA was adapted, capturing the key mechanical and electrical components responsible for generating the damping force. The control voltage was expressed as a function of the damping ratio, stiffness, velocities of the frame and mass, along with the electronic parameters such as inductance, resistance, and the actuator's force constant. A comparison between the simulated and experimentally observed voltages for the passive cases revealed discrepancies, which were analyzed by determining the appropriate scale factor. This attempt aims to improve the accuracy of the system's dynamic response and lower the model-form uncertainty. However, the scaling factor is purely empiric by observation, without any physical explanation yet. Future work will investigate the discrepancy between the experimental and the modelled outcome of the control voltage to find a rather physical explanation.

References

1. Roy, C.J. and Oberkampf, W.L. "A comprehensive framework for verification, validation, and uncertainty quantification in scientific computing". *Computer Methods in Applied Mechanics and Engineering*, 200(25):2131–2144 (2011)
2. Platz, R. "Comprehensive testing environment to evaluate approaches in uncertainty quantification for passive and active vibration isolation". In Mao, Z., editor, *Model Validation and Uncertainty Quantification, Volume 3*, pages 97–106, Cham (2023) Springer International Publishing.
3. Lenz, J. and Platz, R. "Quantification and evaluation of parameter and model uncertainty for passive and active vibration isolation". In Barthorpe, R., editor, *Model Validation and Uncertainty Quantification, Volume 3*, pages 135–147, Cham (2020) Springer International Publishing.
4. Mohan Kumar, M. and Platz, R. "Deterministic and probabilistic comparison of the discrepancy between the numerical simulation and experimental test considering passive and active vibration isolation". In *Proceedings of the International Conference on Uncertainty in Structural Dynamics USD2024 in conjunction with ISMA2024* (2024)
5. Kim, M., Park, J., and Gweon, D. "Mathematical modeling and design considerations for designing voice coil motor". In *Proceedings International Conference on Mechanics, Materials and Structural Engineering (2016)* (2016)
6. Banik, R. and Gweon, D.G. "Design and optimization of voice coil motor for application in active vibration isolation". *Sensors and Actuators A: Physical*, 137(2):236–243 (2007)
7. Yun-Hui, L. and Wei-Hao, W. "Active vibration isolation using a voice coil actuator with absolute velocity feedback control". *International Journal of Automation and Smart Technology*, 3:221–226 (2013)
8. Chi, W., Cao, D., and Huang, W. "An observer-based active vibration isolation system using the voice-coil actuator". *Advanced Materials Research*, 846-847:161–166 (2013)
9. Perfetto, S., Rohlfing, J., Infante, F., Mayer, D., and Herold, S. "Test rig with active damping control for the simultaneous evaluation of vibration control and energy harvesting via piezoelectric transducers" (2016)
10. Ida, N. *The Static Magnetic Field*, pages 377–418. Springer International Publishing, Cham (2021)